Behavior of electron gas in selectively doped GaAs/$Al_xGa_{1-x}As$ multiple-quantum-well structures by Raman scattering

Tonao Yuasa* and Makoto Ishii†
Optoelectronics Joint Research Laboratory, 1333 Kamikodanaka, Nakahara-ku, Kawasaki 211, Japan
(Received 10 April 1987; revised manuscript received 28 September 1987)

Two-dimensional (2D) and three-dimensional (3D) behavior of electron gas (plasmons) in selectively doped GaAs/$Al_xGa_{1-x}As$ multiple-quantum-well (MQW) structures have been studied in detail with the use of Raman scattering, utilizing coupled plasmon–LO-phonon modes as an indication of the dimensionality of the plasmons. Raman scattering was measured at room temperature for two types of the MQW structures in which each well is either doped or modulation doped with electrons. Two Raman modes are observed besides the LO-phonon peaks in the spectra, and the modes are assigned to the intersubband quasi-2D plasmons coupled with LO phonons due to the dependence of the peak frequencies on the well thickness and the electron density. Charge transfer from the $Al_xGa_{1-x}As$ barriers into the wells in the modulation-doped MQW structure is established by comparing the Raman spectrum of the MQW structure with that of the thick $Al_xGa_{1-x}As$ reference layer with the same Al content and doping density as those of barriers. Also, transition from quasi-2D to 3D character of the plasmons with decreasing barrier thickness is discussed on the shifts of the frequencies of the coupled intersubband-plasmon–LO-phonon modes to those of the coupled 3D-plasmon–LO-phonon modes.

I. INTRODUCTION

There has been increased interest in the physical properties of the electron system which is confined at the single interface of heterojunctions and in the potential well of layered heterojunctions. The discrete energy levels are formed by the quantization effects of the confining wells in these systems because of the band-gap discontinuities between the two different materials.[1] The confined electrons are in quantized levels for motion along the direction perpendicular to the heterojunction but are free to move in a plane parallel to the heterointerface. The behavior of the electrons is similar to that of an idealized two-dimensional (2D) electron gas (plasmons).[2–4] The quasi-2D electron gas has been extensively studied in the modulation-doped GaAs/$Al_xGa_{1-x}As$ superlattice system because of the possibility of achieving very high mobility.[5,6] In the modulation-doped system, the charge carriers are transferred from the donors of the selectively doped $Al_xGa_{1-x}As$ layers into the energetically lower conduction band of the GaAs layers, giving rise to a depletion of the electrons in the $Al_xGa_{1-x}As$ layers and to accumulation in the GaAs layers. The electron mobility can be increased by the reduced ionized impurity scattering due to the spatial separation of the ionized donors and the mobile electrons.

Experimental studies of the quasi-2D plasmons have been carried out by means of transport, magnetic transport,[1,7] and optical measurements such as far-infrared absorption[8,9] and light scattering.[10–12] Among these methods, inelastic light scattering is useful for the investigation of the elementary excitations as a spectroscopic tool. Burstein, Pinczuk, and Mills[13] have theoretically discussed inelastic light scattering by charge carrier excitations in 2D plasmas, and have pointed out the high sensitivity of resonant inelastic light scattering for the single particle and collective charge excitations of the layered plasmas. Their predictions were confirmed experimentally by the observation of light scattering from intrasubband and intersubband plasmons at GaAs/$Al_xGa_{1-x}As$ heterostructures.[11,12]

As is well known, plasmons are coupled to longitudinal-optical (LO) phonons in polar semiconductors.[14] The coupling between three-dimensional (3D) plasmons and LO phonons has been studied by Raman scattering in ZnS-type binary alloys such as *n*-type GaAs (Ref. 15), *n*-type InP (Ref. 16), and *p*-type GaAs.[17,18] The 3D-plasmon–LO-phonon coupling has also been measured in the mixed crystals of *n*-type $Al_xGa_{1-x}As$ (Refs. 19 and 20) and *p*-type $Al_xGa_{1-x}As$ (Ref. 18). In degenerate binary semiconductors, two coupled 3D-plasmon–LO-phonon modes denoted by $L_\pm$ participate in the Raman scattering.[21] The third Raman line denoted by L_0 has been observed in the above ternary mixed crystals.[18–20] The frequencies and dampings of the coupled modes depend on the carrier concentration, wave vector, and the alloy composition for the mixed crystals.

The coupling between intersubband plasmons and LO phonons has been found in the low-temperature polarized spectra of GaAs/$Al_xGa_{1-x}As$ heterostructures with layered electron gas, which were measured by resonant inelastic-light scattering.[11,12,22,23] In the measurements, the excitation photon energy was close to the energy separation between the spin-orbit split valence band and the lowest conduction band at the Γ point. In the depolarized spectra, a peak due to spin-flip single-particle intersubband excitation has been observed.[11,12] In addition, intrasubband quasi-2D plasmon like the idealized 2D

plasmon has also been observed in the spectra with the excitation energy close to the lowest conduction-band energy.[24]

As mentioned above, inelastic light scattering is a versatile method for the investigation of electron gas at semiconductor interfaces. The behavior of 2D plasmons is quite different from that of 3D plasmons.[13,25,26] Using the experimental results of 3D plasmons in $Al_xGa_{1-x}As$ and quasi-2D plasmons in GaAs, it is possible to analyze the behavior of electron gas in the $GaAs/Al_xGa_{1-x}As$ layered structures.

In this paper, we study in detail the coupled intersubband-plasmon–LO-phonon modes in doped and modulation-doped $GaAs/Al_xGa_{1-x}As$ multiple-quantum-well (MQW) structures by Raman scattering at room temperature. The assignment to the coupled modes is performed on the peak frequencies in the spectra from the MQW structures with different well thicknesses and electron densities. By comparing these results with Raman spectra from a thick n-type $Al_xGa_{1-x}As$ layer, charge transfer from doped $Al_xGa_{1-x}As$ barriers into undoped GaAs wells is demonstrated spectroscopically. In addition, transition of the dimensionality of the plasmons by reducing the barrier thickness is investigated using the doped MQW structures with differently separated wells. Since the intersubband plasmons can propagate along the heterointerfaces via the long-range Coulomb interaction alone, the plasmons are strongly damped for the propagation.[26] We have successfully observed the coupled intersubband-plasmon–LO-phonon modes in the room-temperature Raman spectra by employing heavily doped MQW structures.

This paper is organized as follows. In the next section the experimental procedure is described. In Sec. III we analyze the coupled intersubband-plasmon–LO-phonon modes. In Sec. IV experimental results are presented and discussed. We conclude in Sec. V by summarizing our results.

II. EXPERIMENT

The $GaAs/Al_xGa_{1-x}As$ MQW structures were grown on Cr-doped (001) semi-insulating GaAs substrates by molecular-beam epitaxy using a Varian MBE GEN II system. The system provides multilayer structures with well-defined layers ranging from as thin as a few monolayers to as thick as hundreds of angstroms. The excellent uniformity in layer thickness, doping, and alloy composition over a large area is reproducibly obtainable by precisely controlling beam fluxes and rotating the substrate holder.

The MQW structures were accompanied with the thick Si-doped n-type GaAs and $Al_xGa_{1-x}As$ layers named reference layers to estimate the electron densities and the alloy compositions in the MQW structures. An $\sim$0.5-μm-thick undoped GaAs buffer layer was first grown on the substrate. After a 1.0–1.5-μm-thick Si-doped n-type $Al_xGa_{1-x}As$ reference layer, an $\sim$0.5-μm-thick Si-doped n-type GaAs reference layer, a 1.0–1.5-μm-thick undoped $Al_xGa_{1-x}As$ layer, and 0.3–0.5-μm-thick MQW structures were successively grown at a substrate temperature of 700–730 °C. Two types of selectively doped MQW structures were constructed. One is the doped MQW in which wells are selectively doped with Si. The other is the modulation-doped MQW in which barriers are selectively doped with Si. The well thickness (L_Z) ranges from 110 to 150 Å, and the barrier thickness (L_B) ranges from 10 to 70 Å. In order to obtain an unchanged Al content in the $Al_xGa_{1-x}As$ barrier and reference layers, and keep the doping density in the MQW and the reference layers at constant the temperatures of Ga, As, Al, and Si sources were fixed during growth. The Al content was 0.2–0.3, and the doping density was 2×10^{18}–4×10^{18} cm^{-3}.

The Raman experiments have been performed in the usual backscattering configuration at room temperature. The 488.0- and 514.5-nm lines of a Spectra Physics model 164 Ar-ion laser were used as exciting light sources. The results presented are those obtained with the 514.5-nm line (0.2–0.3 W). The diameter of the laser beam on the samples was focused to about 200 μm. The scattered light was analyzed with a Jobin-Ybon RAMANOR U-1000 double monochromator with a resolution of 0.4 cm^{-1}, and detected by a cooled RCA GaAs photocathode-type photomultiplier equipped with photon-counting electronics. The detected counts were stored in a Tracor Northern TN-1710 multichannel analyzer with typical integration time of 0.4 s and then recorded on an X-Y plotter.

III. THEORY

The frequencies of the coupled intersubband-plasmon–LO-phonon modes in a selectively doped MQW heterostructure are determined by the zero of the real part of the dielectric function.[13,27,30] The coupled modes between different wells interact through the Coulomb force. If we assume that only the ground subband is occupied by electrons, as is usually the case experimentally, and consider only the transition between the first excited subband and the ground subband, the dielectric function of the MQW structure is described in the following form:[13]

$$\epsilon(\omega)=\epsilon_\infty+\frac{\epsilon_0-\epsilon_\infty}{1-\omega^2/\omega_t^2}-\frac{\omega_p^{*2}\epsilon_\infty}{\omega^2-\omega_{01}^2}\ , \tag{1}$$

where ω_t is the transverse-optical (TO) -phonon frequency, ϵ_∞ is the high-frequency dielectric constant, $\epsilon_0=\omega_l^2/\omega_t^2$ is the static dielectric constant (ω_l is the LO-phonon frequency), ω_{01} is the subband splitting between the first excited subband and the ground subband, and ω_p^* is the effective plasma frequency. In Eq. (1),

$$\omega_p^{*2}=\frac{2n_s\omega_{01}}{\hbar}V_{01}\ , \tag{2}$$

where V_{01} is the Coulomb interaction for the ground and the first excited subbands between different quantum wells, and n_s is the electron density in each quantum well.

For small in-plane and infinite normal components of the wave vector in which layering effects dominate,

$$V_{01} \simeq \frac{2\pi e^2 L_{01}}{\epsilon_\infty} \times \left[1 - \frac{q_\parallel^2 Z_{01}^2 (1 - e^{-2q_\parallel d})}{L_{01}[1 - 2e^{-q_\parallel d}\cos(q_\perp d) + e^{-2q_\parallel d}]} \right] \simeq \frac{2\pi e^2 L_{01}}{\epsilon_\infty} \left[1 - \frac{q_\parallel^2 Z_{01}^2 d}{L_{01}} \frac{1}{1 - \cos(q_\perp d)} \right] \quad (q_\parallel d \to 0) , \tag{3}$$

where L_{01} is the Coulomb integral of the wave functions of the ground and the first excited subbands, Z_{01} is the dipole matrix element, and $q_\parallel$ and $q_\perp$ are the in-plane and normal components of the wave vector, respectively.[26] From the condition $\epsilon(\omega)=0$, we obtain the frequencies of the coupled modes $I_\pm$:

$$\omega_{i\pm}^2 = \tfrac{1}{2}(\omega_{01}^2 + \omega_l^2 + \omega_p^{*2}) \pm \tfrac{1}{2}[(\omega_{01}^2 + \omega_l^2 + \omega_p^{*2})^2 - 4(\omega_{01}^2\omega_l^2 + \omega_t^2\omega_p^{*2})]^{1/2} . \tag{4}$$

Intersubband excitations are shifted to higher energies because of depolarization effects.[31,32] The shifted excitations are given by

$$\omega_{01}^{*2} = \omega_{01}^2 + \omega_p^{*2} . \tag{5}$$

Equations (2) and (4) indicate that $\omega_{i\pm}$ depend on both ω_{01} and ω_p^*, i.e., well thickness and electron density.

Figure 1 shows the calculated $\omega_{i\pm}$ in GaAs/$Al_{0.2}Ga_{0.8}As$ MQW structures with a constant $n_s = 1\times10^{12}$ cm^{-2} as a function of ω_{01}. In the calculation, L_{01} is roughly approximated to depend linearly on L_Z with the relation of $L_{01}\sim 0.11 L_Z$ (Å).[26] With increasing ω_{01}, the I_+ mode shifts from the LO-phonon frequency position to the higher frequency side and the I_- mode approaches the LO-phonon frequency position from the lower-frequency side, crossing the ω_{01} value at ω_t. At large subband splitting, $\omega_{i+}\sim\omega_p^*$.[13]

The n_s dependence of $\omega_{i\pm}$ is classified into three regimes: the large subband splitting regime ($\omega_{01}\gtrsim\omega_l$), the intermediate subband splitting regime ($\omega_t<\omega_{01}\lesssim\omega_l$), and the small subband splitting regime ($\omega_{01}<\omega_t$). Figure 2 shows how $\omega_{i\pm}$ and ω_{01}^* change with increasing n_s for GaAs/$Al_{0.2}Ga_{0.8}As$ MQW with $\omega_{01}=15$, 35, and 40 meV. In the regime $\omega_{01}\gtrsim\omega_l(=36$ meV), the I_+ mode shifts from ω_{01} to the higher-frequency side, the I_- mode shifts from ω_l to ω_t, and $\omega_t\sim\omega_{01}^*$ in the wide range of n_s. In the regime $\omega_t(=33$ meV$)<\omega_{01}\lesssim\omega_l$, the I_+ mode starts from ω_l for the higher frequency side, the I_- mode shifts from ω_{01} to ω_t, and $\omega_{i-}\sim\omega_{01}^*$ in the limit of small n_s and $\omega_{i+}\sim\omega_{01}^*$ in the limit of large n_s. In the regime $\omega_{01}<\omega_t$, the I_- mode shifts for the higher frequency side from ω_{01} to ω_t, and ω_{01}^* approaches ω_{i+} from ω_{i-}.

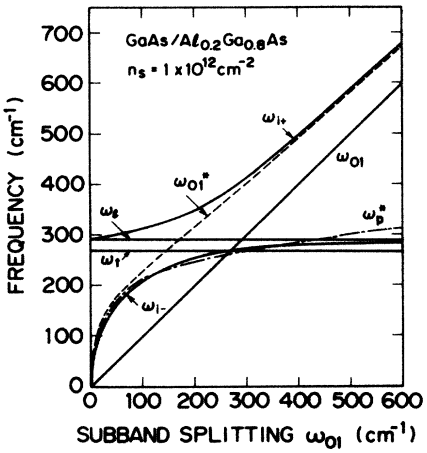

FIG. 1. Calculated shifts of the frequencies $\omega_{i\pm}$ of the coupled intersubband-plasmon–LO-phonon modes $I_\pm$ in a GaAs/$Al_{0.2}Ga_{0.8}As$ MQW structure ($L_Z=200$ Å and $n_s=1\times10^{12}$ cm^{-2}) as a function of the subband splitting ω_{01}. The effective plasmon frequency ω_p^* and the depolarization field subband splitting ω_p^* are also given. The frequencies of the LO and TO phonons in GaAs are denoted by ω_l and ω_t, respectively.

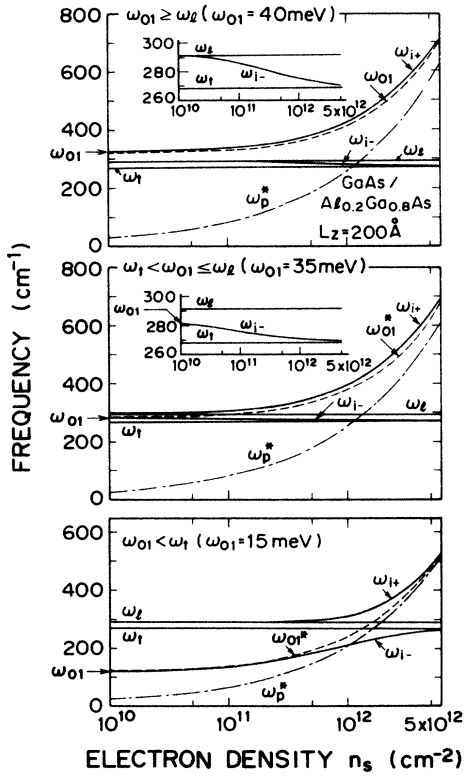

FIG. 2. The dependence of the calculated frequencies $\omega_{i\pm}$ of the coupled intersubband-plasmon–LO-phonon modes in a GaAs/$Al_{0.2}Ga_{0.8}As$ MQW structure ($L_Z=200$ Å) on the electron density n_s. The subband splitting ω_{01} is classified into three regions: $\omega_{01}\gtrsim\omega_l$, $\omega_t<\omega_{01}<\omega_l$, and $\omega_{01}<\omega_t$.

IV. RESULTS AND DISCUSSIONS

A. Coupled intersubband-plasmon–LO-phonon modes

Figure 3(a) shows the Raman spectrum from an undoped GaAs/$Al_{0.20}Ga_{0.80}As$ MQW heterostructure ($L_Z \sim 150$ Å, $L_B \sim 50$ Å). Above five periods in the MQW structure are excited by the incident laser light with the penetration depth of ~ 1000 Å. Three LO-phonon peaks, one denoted LO at 291 cm^{-1} and two others denoted GaAs-LO at 282 cm^{-1} and AlAs-LO at 373 cm^{-1}, are observed in the undoped sample. The LO represents the LO phonons of pure GaAs, the GaAs-LO and the AlAs-LO represent two branches of the LO phonons of $Al_{0.2}Ga_{0.8}As$. In contrast, two additional peaks denoted $I_\pm$ appear in the spectrum from the doped GaAs/$Al_{0.2}Ga_{0.8}As$ structure ($n_s \sim 3\times 10^{12}$ cm^{-2}) in Fig. 3(b). The value of n_s was estimated from L_Z and the carrier concentration n in the thick n-type GaAs reference layer, where n was determined by the frequencies of the coupled 3D-plasmon–LO-phonon modes.[15] The I_+ mode (625 cm^{-1}) at the higher frequency side is broad and weak, and the I_- mode (273 cm^{-1}) at the lower frequency side is close to the peak of GaAs-like LO phonons of $Al_{0.2}Ga_{0.8}As$ (Ref. 33), as seen in Fig. 3(b). The $I_\pm$ modes are also observed in the modulation-doped MQW structure. Figures 4(a) and 4(b) show the Raman spectra from an undoped and a modulation-doped GaAs/$Al_{0.27}Ga_{0.73}As$ MQW structure ($L_Z \sim 130$ Å, $L_B \sim 70$ Å), respectively. The features of the I_+ (745 cm^{-1}) and I_- (276 cm^{-1}) modes in Fig. 4(b) are very similar to those in Fig. 3(b).

The comparison of the spectra of the selectively doped MQW [Figs. 3(b) and 4(b)] with those of the undoped MQW [Figs. 3(a) and 4(a)] indicates that the $I_\pm$ modes are induced by the degenerate quasi-2D carriers in the GaAs wells. Figure 5 shows the Raman spectra from a modulation-doped MQW structure excited by two different laser lines. The sample is the same as the one used for Fig. 4(b). When the wavelength of the excitation line is changed from 514.5 to 488.0 nm, the frequencies of the I_+ and I_- modes shift to the higher frequency side by 8 and 0.8 cm^{-1}, respectively, and the damping of the I_+ mode increases from ~ 130 to ~ 150 cm^{-1}. This wave-vector-dependent behavior leads to an interpretation of the $I_\pm$ modes as the two branches of the coupled quasi-2D-plasmon–LO-phonon modes.[26] Furthermore, it is noted that the I_- mode in Figs. 3(b) and 4(b) exists at the position between the LO (291 cm^{-1}) and TO (268 cm^{-1}) phonons. The frequency position is forbidden for the coupled 2D-plasmon–LO-phonon modes with a smaller wave vector,[14,15,34] but it is allowed for the coupled intersubband-plasmon–LO-phonon modes in the wells with the subband splitting ω_{01} larger than ω_t, as shown in Fig. 2. The splitting energies for Figs. 3(b) and 4(b) are evaluated to be 374 and 477 cm^{-1}, respectively, and these values are larger than ω_t. Accordingly, the I_- mode is assigned to the lower branch of the coupled intersubband-plasmon–LO-phonon modes. The I_+

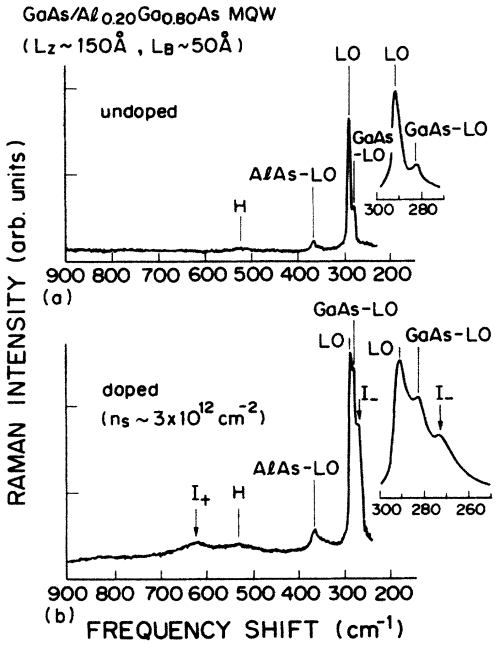

FIG. 3. Raman spectra of (a) an undoped and (b) a doped GaAs/$Al_{0.2}Ga_{0.8}As$ MQW structure with $L_Z \sim 150$ Å and $L_B \sim 50$ Å. The arrows denoted $I_\pm$ represent the coupled intersubband-plasmon–LO-phonon modes. The lines denoted LO, GaAs-LO, and AlAs-LO are the LO phonon of pure GaAs and the GaAs and AlAs-like modes of the LO phonons in $Al_xGa_{1-x}As$, respectively. Some broad peaks denoted H are the second-order phonon modes.

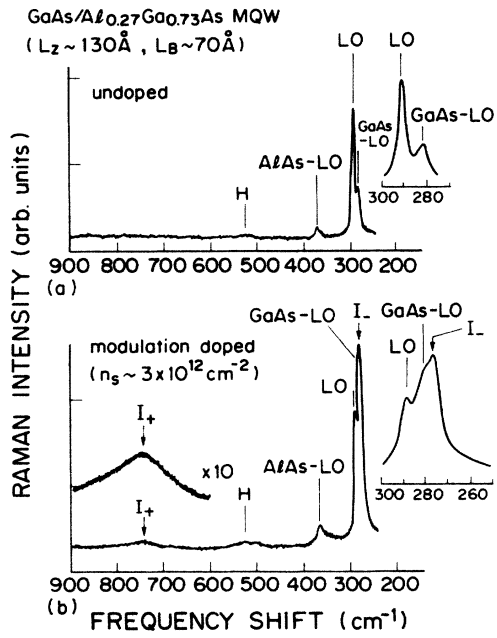

FIG. 4. Raman spectra of (a) undoped and (b) modulation-doped GaAs/$Al_{0.27}Ga_{0.73}As$ MQW structures with $L_Z \sim 130$ Å and $L_B \sim 70$ Å.

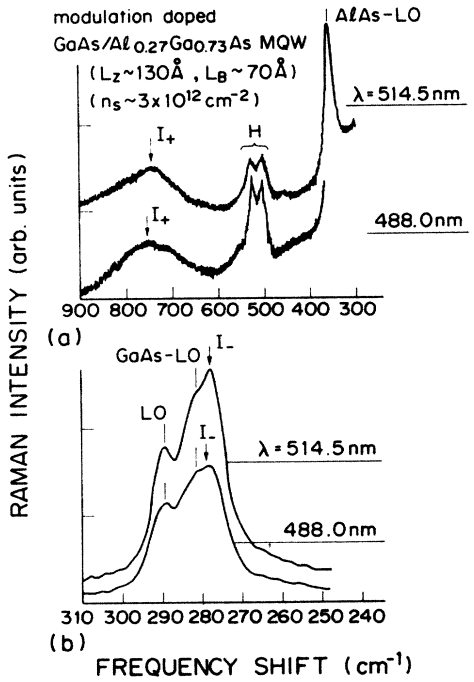

FIG. 5. Raman spectra of a modulation-doped GaAs/$Al_{0.27}Ga_{0.73}As$ MQW structure at two different laser-excitation wavelengths (λ). The spectra are shown in (a) the high-frequency and (b) the low-frequency ranges. The sample is the same as that for Fig. 4(b).

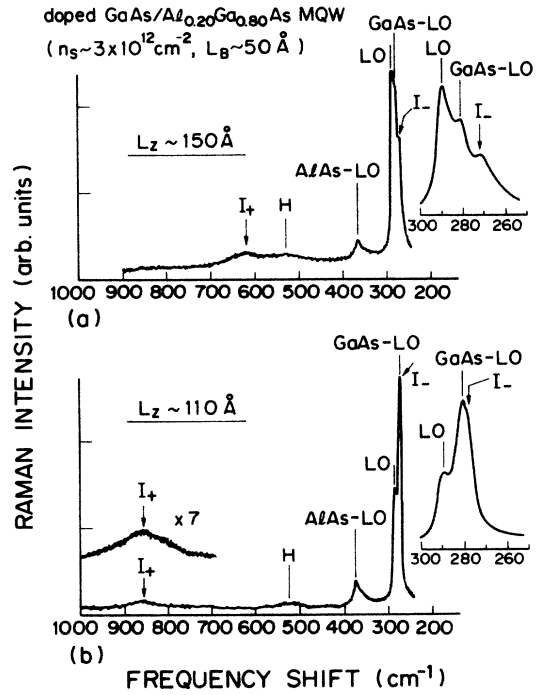

FIG. 6. Raman spectra of doped GaAs/$Al_{0.20}Ga_{0.80}As$ MQW structures with (a) $L_Z \sim 150$ Å and (b) ~ 110 Å. L_B and n_s are fixed at ~ 50 Å and $\sim 3\times 10^{12}$ cm^{-2}, respectively. The sample with $L_Z \sim 150$ Å is the same as that for Fig. 3(b).

mode corresponds to the upper branch of the coupled modes. The LO-phonon peaks in Figs. 3(b), 4(b), and 5 originate from the depletion layers.

In order to confirm the above-described assignment to the coupled mode, we have examined dependence of the $I_{\pm}$ modes on both the subband splitting ω_{01} and the electron density n_s, which is analyzed in Sec. III. ω_{01} changes sensitively with I_Z. The spectra of two different MQW structures with selectively doped ~ 150-Å- and ~ 110-Å-thick wells are compared in Fig. 6. L_B and n_s are fixed at ~ 50 Å and $\sim 3\times 10^{12}$ cm^{-2}, respectively, for the two structures. The sample with $L_Z \sim 150$ Å is the same as that is used for Fig. 3(b), and it is also used for Fig. 7, as described below. Figure 6 shows also the expanded spectra for the neighborhood of the LO phonons of GaAs and $Al_{0.2}Ga_{0.8}As$. The $I_{\pm}$ modes for $L_Z \sim 150$ Å are clearly observed with a distinct separation from the AlAs-like and the GaAs-like LO-phonon peaks, respectively, while for $L_Z \sim 110$ Å the I_+ mode weakens and the I_- mode appears as a shoulder close to the GaAs-like LO phonons. Changes in the frequencies of the coupled modes are apparent, as shown in Fig. 6. When L_Z decreases from 150 to 110 Å, the I_+ mode shifts markedly to the higher-frequency side by 215 cm^{-1} from 630 to 845 cm^{-1}, and the I_- mode shifts by 6 cm^{-1} from 273 to 279 cm^{-1}. The measured frequency shifts to the higher-frequency side with decreasing well thickness, i.e., increasing subband splitting, are agreement with the results predicted theoretically in Fig. 1.

As illustrated in Figs. 2, ω_{i-} increases with n_s in the MQW structures with a given $\omega_{01} < \omega_t$, but on the contrary ω_{i-} decreases with increasing n_s in the MQW structures with $\omega_{01} > \omega_t$. Figure 7 shows the spectra of doped GaAs/$Al_{0.20}Ga_{0.80}As$ MQW structures with different n_s (3×10^{12} and 5×10^{12} cm^{-2}) and a fixed dimension of $L_Z \sim 150$ Å and $L_B \sim 50$ Å. The value of ~ 370 cm^{-1} is larger than ω_t. The I_+ modes shift to the higher-frequency side from 625 to 711 cm^{-1} with increasing n_s. In contrast, the I_- mode shifts to the lower-frequency side from 273 to 270 cm^{-1}, and appears clearly at $n_s \sim 5\times 10^{12}$ cm^{-2} [Fig. 7(b)]. Thus, the change in n_s agrees well with the theoretical predictions.

Above experimental data confirm that the two additional modes denoted $I_{\pm}$ in the Raman spectra of doped and modulation-doped GaAs/$Al_xGa_{1-x}As$ MQW structures with high electron densities are the coupled intersubband-plasmon–LO-phonon modes. In the following sections, these results are applied to study the charge transfer from barriers into wells and the transition of dimensionality of electron gas with decreasing barrier thickness in the GaAs/$Al_xGa_{1-x}As$ MQW structures.

B. Charge transfer from barriers into wells

The potential barrier at the interface between GaAs and $Al_xGa_{1-x}As$ layers occurs mainly in the conduction band, and therefore the bottom of the conduction band in the GaAs layer is lower energetically than the shallow

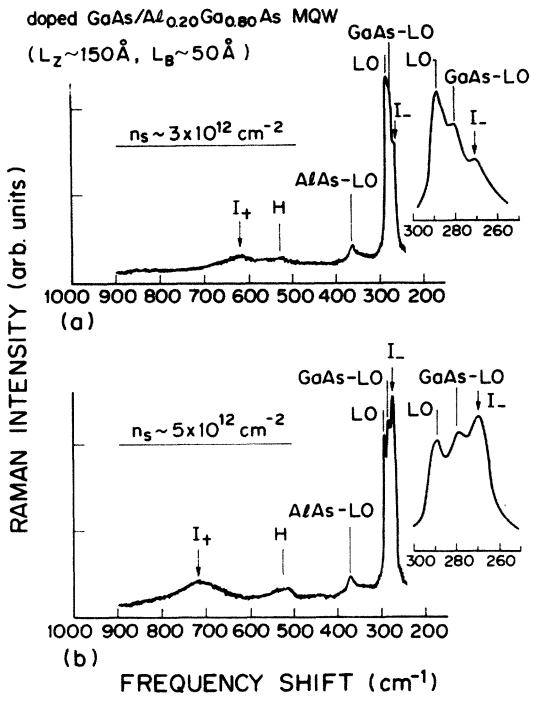

FIG. 7. Raman spectra of doped $GaAs/Al_{0.20}Ga_{0.80}As$ MQW structures with (a) $n_s \sim 3\times10^{12}$ cm^{-2} and (b) $\sim 5\times10^{12}$ cm^{12}. $L_Z \sim 150$ Å and $L_B \sim 50$ Å. The sample with $n_s \sim 3\times10^{12}$ cm^{-2} is the same as that for Figs. 3(b) and 6(a).

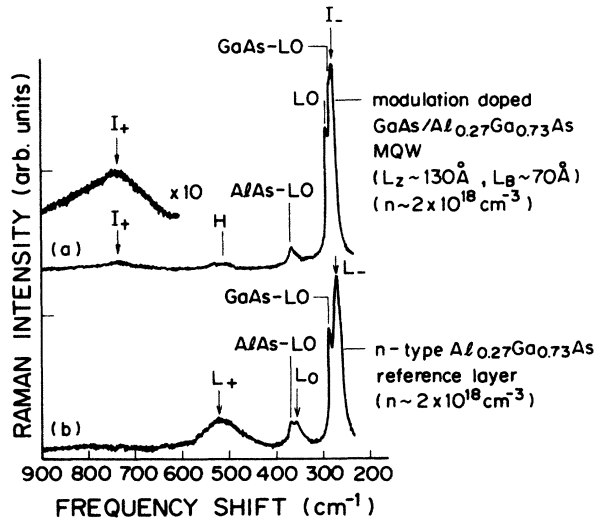

FIG. 8. Raman spectra of a modulation-doped $GaAs/Al_{0.27}Ga_{0.73}As$ MQW structure ($L_Z \sim 130$ Å and $L_B \sim 70$ Å) and a n-type $Al_{0.27}Ga_{0.73}As$ reference layer. The MQW and n-type $Al_{0.27}Ga_{0.73}As$ reference layer are doped with the same Si doping density ($n \sim 2\times10^{18}$ cm^{-3}). The arrows denoted $L_\pm$ and L_0 represent the coupled 3D-plasmon–LO-phonon modes.

donor state in the $Al_xGa_{1-x}As$ layer.[1] Such an energy difference causes a transfer of charge carriers from the shallow donors of the barriers into the wells in a modulation-doped $GaAs/Al_xGa_{1-x}As$ MQW structure. As a result, the barriers are depleted and the electrons are accumulated in the wells. The 2D character of the accumulated electrons are demonstrated by Shubnikov–de Haas measurements.[35,36] In this section, we analyze spectroscopically the charge transfer using the above Raman results.

Figures 8(a) and 8(b) show the Raman spectra of a modulation-doped $GaAs/Al_{0.27}Ga_{0.73}As$ MQW ($L_Z \sim 130$ Å and $L_B \sim 71$ Å) and a 1.5-μm-thick Si-doped n-type $Al_{0.27}Ga_{0.73}As$ reference layer, respectively. The spectra in the frequency range below 500 cm^{-1} are enlarged in Fig. 9. Since the MQW and the reference layer were grown successively on the same substrate under the fixed beam fluxes of Al, Ga, As, and Si during growth, the Al content and Si doping density are the same as those in the $Al_{0.27}Ga_{0.73}As$ reference layer. In Fig. 8(a) the coupled intersubband-plasmon–LO-phonon modes $I_\pm$ are observed at 745 and 276 cm^{-1}, respectively, besides the LO-phonon peaks, as identified in the above section. On the other hand, in Fig. 8(b) three additional peaks denoted $L_\pm$ and L_0 are observed besides the two LO-phonon branches of $Al_{0.27}Ga_{0.73}As$. The frequencies of the LO-phonon peaks of $Al_xGa_{1-x}As$ are coincident in Fig. 8, showing the same alloy composition of the barriers and the reference layer. The frequency of the broad L_+ mode is much higher than that of the AlAs-like LO phonons (377 cm^{-1}), and the frequencies of the sharper L_0 and L_- modes are close to those of AlAs-like (360 cm^{-1}) and GaAs-like TO (266 cm^{-1}) phonons. These characteristics lead to the assignment of the $L_\pm$ and L_0 modes to the three branches of the coupled 3D-plasmon–LO-phonon modes.[19,20] The carrier concentration in the reference layer is determined to be $\sim 2\times10^{18}$ cm^{-3} from the peak frequency of the L_+ mode.[20] Although the barriers have the same Si doping density as that in the $Al_{0.27}Ga_{0.73}As$ reference layer, the $L_\pm$ and L_0

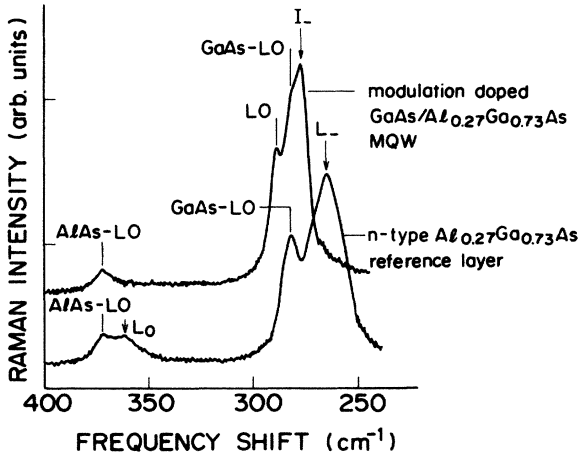

FIG. 9. Spectra in Fig. 8 are expanded for the frequency range below 400 cm^{-1}.

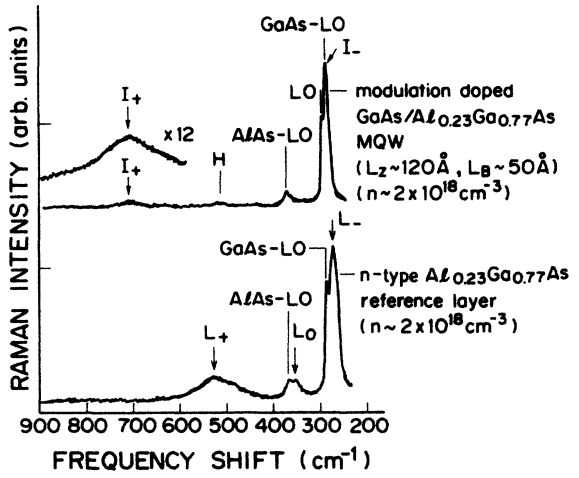

FIG. 10. Raman spectra of a modulation-doped $GaAs/Al_{0.23}Ga_{0.77}As$ MQW structure ($L_Z \sim 120$ Å and $L_B \sim 50$ Å) and a n-type $Al_{0.23}Ga_{0.77}As$ reference layer. The MQW and n-type $Al_{0.23}Ga_{0.77}As$ reference layer are doped with the same Si doping density ($n \sim 2\times 10^{18}$ cm^{-3}).

modes vanish completely in the spectrum of the MQW structure, as shown in Figs. 8(a) and 9. If the electrons in the barriers partly transfer into the wells, and the electrons remain in the barriers, the coupled modes should shift to the lower-frequency side.[15,34] However, no indications of the three branches of the coupled 3D-plasmon–LO-phonon modes were observed in the frequency range below 500 cm^{-1}. This means that the electrons are transferred from the Si donors in the barriers into the wells with the complete depletion of the barriers, and the accumulated electrons exhibit the 2D character.

The other example of the charge transfer is shown in Figs. 10 and 11. The spectrum of the ~ 1.0-μm-thick $Al_{0.21}Ga_{0.19}As$ reference layer shows clearly the $L_\pm$ and L_0 modes. On the other hand, for the modulation-doped

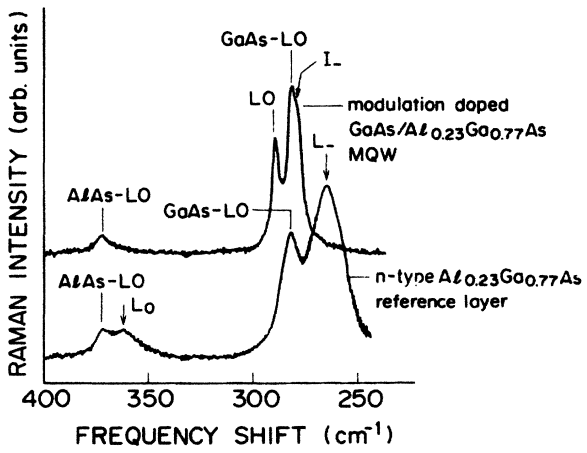

FIG. 11. Spectra in Fig. 10 are expanded for the frequency range below 500 cm^{-1}.

MQW structure, the coupled 3D-plasmon–LO-phonon modes vanish and instead the $I_\pm$ modes appear, as shown in Figs. 10(a) and 11. The broad I_+ mode peaks at the high frequency of 710 cm^{-1}, and the I_- mode appears at 279 cm^{-1} as a shoulder close to the GaAs-like LO phonons.

As described above, the transfer of electrons between the barriers and the wells are spectroscopically established by the disappearance of the 3D plasmons and the appearance of the quasi-2D plasmons through the coupling with the LO phonons.

C. Transition of dimensionality of quasi-2D electron gas

When the separation between the adjacent wells is very small, the wave functions of electrons overlap between the wells, resulting in the formation of broad energy instead of quantum states. For the small separation between wells, the behavior of plasmons becomes effectively three-dimensional.[37] The transition from quasi-2D to 3D behavior of the plasmons is expected to be observed in the Raman spectra as the change in the frequencies of the coupled plasmon–LO-phonon modes.

Figure 12 shows the Raman spectra of two types of doped $GaAs/Al_{0.20}Ga_{0.80}As$ MQW structures with $L_Z \sim 100$ Å and different barrier thickness ($L_B \sim 10$ Å and ~ 50 Å), and of a 0.5-μm-thick Si-doped n-type GaAs reference layer. The spectra in the lower-frequency range in Fig. 12(a) are enlarged in Fig. 12(b).

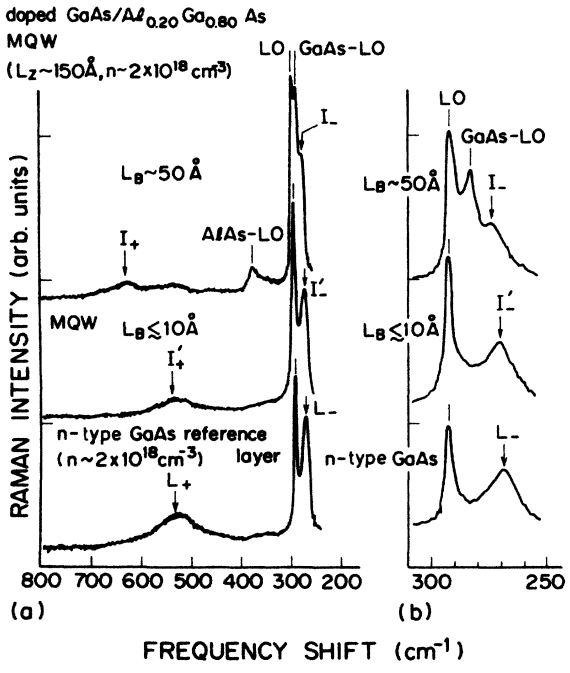

FIG. 12. (a) Raman spectra of a doped $GaAs/Al_{0.20}Ga_{0.80}As$ MQW structure ($L_Z \sim 150$ Å) with $L_B \sim 50$ Å and $\lesssim 10$ Å, and an n-type GaAs reference layer. The two MQW structures and the n-type GaAs reference layer are doped with the same Si doping density ($n \sim 2\times 10^{18}$ cm^{-3}). (b) Expanded spectra for the lower-frequency range of Fig. 12(a).

The three sample structures were grown successively on the same substrate and the Si doping density was kept at constant ($n \sim 2\times10^{18}$ cm^{-3}) in the structures. For the MQW structure with $L_B \sim 50$ Å, the coupled intersubband-plasmon–LO-phonon modes $I_\pm$ are seen at 625 and 274 cm^{-1}, respectively. In the quantum wells where the alloy composition of the barrier and n_s are fixed, $\omega_{i\pm}$ should be unchanged for different barrier thickness, because $\omega_{i\pm}$ have no dependence on barrier thickness, as indicated in Eqs. (2)–(5). However, for the very thin barrier ($L_B \lesssim 10$ Å), although the doping density is the same value as that in the MQW structure with $L_B \sim 50$ Å, the coupled modes shift to the lower frequencies of $\sim$550 and 270 cm^{-1}, respectively, as denoted by $I'_\pm$ in Fig. 12. In addition, the frequencies of $I'_\pm$ modes are nearly equal to those of the 3D-plasmon–LO-phonon coupled modes $L_\pm$ in the thick n-type GaAs layer with the same doping density (the frequencies of the $L_\pm$ modes in Fig. 12 are 544 and 268 cm^{-1}). These results suggest that the $I'_\pm$ modes are due to the coupling between the 3D-like plasmons propagating across the barriers and the LO phonons. This interpretation is supported by a theoretical result, as discussed below. Theoretical calculation on a Kroning-Penny-type model shows that $Al_{0.22}Ga_{0.78}As$ barriers with the layer thickness less than 25 Å broadens significantly the lowest electronic state in the quantum wells due to the formation of the miniband.[38] The formation of the miniband grows the conduction across the layers and establishes 3D behavior of plasmons. Das Sarma and Quinn have pointed out that the dimensionality of layered electron gas in superlattices changes from 2D to 3D behavior as the coupling between the layers increases with decreasing the quantity $q_\parallel S$, where S is the superlattice period.[38] In the strong coupling ($q_\parallel S \ll 1$) situation, the plasmon is essentially a 3D plasmon, in the weak coupling ($q_\parallel S \gg 1$) situation, the plasmon is a 2D plasmon, and in the intermediate ($q_\parallel S \sim 1$) situation the plasmons of the superlattice have intermediate character between 2D and 3D plasmons. At the excitation wavelength of 514.5 nm, $q_\parallel \approx 0.4\times10^5$ cm^{-1}.[24] Then, for the MQW structure with $L_Z \sim 100$ Å and $L_B \lesssim 10$ Å, $S \lesssim 110$ Å, and therefore $q_\parallel S \lesssim 0.04$. This value of $q_\parallel S$ supports theoretically the 3D character of plasmons in the strong coupling situation for the sample with $L_B \lesssim 10$ Å. Note that the frequencies of the $I_\pm$ modes are not completely in agreement with those of the $L_\pm$ modes, i.e., the $I_\pm$ modes are situated at the slightly higher frequency sides compared with the $I_\pm$ modes. These small differences in the frequencies indicate the slight admixture of 2D character with 3D character in the plasmons, as predicted in the case of the finite $q_\perp S$.[37]

Kirillov, Webb, and Eckstein have recently studied the transformation from quasi-2D to 3D behavior of electron gas in an n-type GaAs/$Al_xGa_{1-x}As$ MQW structure with homogeneous doping of both GaAs and $Al_xGa_{1-x}As$ layers by Raman scattering.[39] They have observed the appearance of the coupled 3D-plasmon–LO-phonon modes in the MQW structure with $L_Z = L_B = 10$–20 Å and 300–5000 Å, and the disappearance of the coupled modes in the structures with $L_Z = L_B = 50$ and 100 Å, and they have conjectured the reappearance of the coupled modes for $L_Z = L_B = 10$–20 Å due to the transition from quasi-2D to 3D character of the plasmons. However, they have found no peaks of the quasi-2D plasmon related modes in the Raman spectra. On the other hand, we have found the quasi-2D intersubband plasmons coupled with the LO phonons for the MQW structure with $L_B \sim 50$ Å, in addition to the 3D plasmons for $L_B \lesssim 10$ Å, as described above. Thus, our results provide a clear evidence of the change in dimensionality of the plasmon with decreasing the barrier thickness.

V. CONCLUSIONS

We have investigated in detail the collective excitations in doped and modulation-doped GaAs/$Al_xGa_{1-x}As$ MQW structures with high electron densities by Raman scattering. The two lines denoted $I_\pm$ were observed besides the LO phonons in the room-temperature spectra for $L_Z = 110$–160 Å and $L_B = 50$–70 Å. The broad I_+ mode is situated at the higher-frequency side, separating from the AlAs-like LO phonons of $Al_xGa_{1-x}As$. On the other hand, the narrower I_- mode is situated at the frequency position between the LO and TO phonons of GaAs, which is forbidden for the coupled 3D-plasmon–LO-phonon modes with small wave vectors. Also, the $I_\pm$ modes have the peak frequencies dependent sensitively on both L_Z and the carrier density, and the modes were assigned to the coupled quasi-2D-intersubband-plasmon–LO-phonon modes on the agreement of the experimental results with the theoretical prediction.

The $I_\pm$ modes were utilized to study charge transfer from Si-doped barriers into undoped wells in modulation-doped MQW structures. The spectra of the MQW structures were compared with those of thick n-type $Al_xGa_{1-x}As$ reference layers with the same Al contents and Si doping densities as those in barriers. Three branches of the coupled 3D-plasmon–LO-phonon modes, which are clearly observed in the $Al_xGa_{1-x}As$ reference layers, disappear in the spectra of the MQW structure and instead the $I_\pm$ modes appear. These results establish spectroscopically the charge transfer from the barriers into the wells.

For a doped MQW structure, the coupled plasmon–LO-phonon modes shift to the lower frequency side with decreasing L_B, when $L_B < 10$ Å, the modes approach the frequencies of the coupled 3D-plasmon–LO-phonon modes in the thick GaAs reference layer with the same doping density as that in the doped wells. The frequency shifts indicate the transformation from quasi-2D to 3D behavior of plasmons when the barrier becomes thin enough to tunnel electrons with strong coupling between wells.

ACKNOWLEDGMENT

The present research is supported by the Agency of Industrial Science and Technology, Ministry of International Trade and Industry, Japan.

*Present address: Opto-Electronics Research Laboratories, NEC Corporation, 4-1-1 Miyazaki, Miyamae-ku, Kawasaki 213, Japan.

†Present address: LSI Research and Development Laboratory, Mitsubishi Electric Corporation, 4-1 Mizuhara, Itami, Hyogo 664, Japan.

[1]R. Dingle, H. L. Störmer, A. C. Gossard, and W. Wiegmann, Surf. Sci. **98**, 90 (1980).

[2]D. A. Dahl and L. J. Sham, Phys. Rev. B **16**, 651 (1977).

[3]P. B. Visscher and L. M. Falicov, Phys. Rev. B **3**, 2541 (1971).

[4]S. Das Sarma and A. Madhukar, Phys. Rev. B **23**, 805 (1981).

[5]R. Dingle, H. L. Störmer, A. C. Gossard, and W. Wiegmann, Appl. Phys. Lett. **33**, 665 (1978).

[6]S. Mori and T. Ando, Surf. Sci. **98**, 101 (1980).

[7]L. L. Chang and L. Esaki, Surf. Sci. **98**, 70 (1980), and references therein.

[8]L. L. Chang, Surf. Sci. **73**, 226 (1978).

[9]R. Dingle, Surf. Sci. **73**, 226 (1978).

[10]P. Manuel, G. A. Sai-Halasz, L. L. Chang, C. A. Chang, and L. Esaki, Phys. Rev. Lett. **37**, 1701 (1976).

[11]G. Abstreiter and K. Ploog, Phys. Rev. Lett. **42**, 1308 (1979).

[12]A. Pinczuk, H. L. Störmer, R. Dingle, J. M. Worlock, W. Wiegmann, and A. C. Gossard, Solid State Commun. **32**, 1001 (1979).

[13]E. Burstein, A. Pinczuk, and D. L. Mills, Surf. Sci. **98**, 451 (1980).

[14]B. Varga, Phys. Rev. **137**, A1896 (1965).

[15]A. Mooradian and G. B. Wright, Phys. Rev. Lett. **16**, 999 (1966).

[16]V. I. Zemski, E. L. Ivchenko, D. M. Mirlin, and I. I. Reshina, Solid State Commun. **16**, 221 (1975).

[17]D. Olego and M. Cardona, Phys. Rev. B **24**, 7217 (1981).

[18]T. Yuasa and M. Ishii, Phys. Rev. B **35**, 3962 (1981).

[19]T. Yuasa, S. Naritsuka, M. Mannoh, K. Shinozaki, K. Yamanaka, Y. Nomura, M. Mihara, and M. Ishii, Appl. Phys. Lett. **46**, 176 (1985).

[20]T. Yuasa, S. Naritsuka, M. Mannoh, K. Shinozaki, K. Yamanaka, Y. Nomura, M. Mihara, and M. Ishii, Phys. Rev. B **33**, 1222 (1986).

[21]M. V. Klein, in *Light Scattering in Solids,* Vol. 8 of *Topics in Applied Physics,* edited by M. Cardona *et al.* (Springer-Verlag, Berlin, 1975), p. 147.

[22]A. Pinczuk and J. M. Worlock, Solid State Commun. **36**, 43 (1980).

[23]R. Sooryakumar, A. Pinczuk, A. Gossard, and W. Wiegmann, Phys. Rev. B **31**, 2578 (1985).

[24]D. Olego, A. Pinczuk, A. C. Gossard, and W. Wiegmann, Phys. Rev. B **25**, 7867 (1982).

[25]W. L. Bloss and E. M. Brody, Solid State Commun. **43**, 523 (1982).

[26]W. L. Bloss, Solid State Commun. **46**, 143 (1983).

[27]A. C. Tsellis and J. J. Quinn, Phys. Rev. B **29**, 3318 (1984).

[28]S. Das Sarma, Phys. Rev. B **29**, 2334 (1984).

[29]G. Fishman, A. Pinczuk, J. M. Worlock, H. L. Störmer, A. C. Gossard, and W. Wiegmann, J. Phys. (Paris) Colloq. **12**, C6-305 (1981).

[30]S. Das Sarma, Appl. Surf. Sci. **11/12**, 535 (1982).

[31]W. P. Chen, Y. J. Chen, and E. Burstein, Surf. Sci. **58**, 263 (1976).

[32]S. J. Allen, Jr., D. C. Tsui, and B. Vinter, Solid State Commun. **20**, 425 (1976).

[33]O. K. Kim and W. G. Spitzer, J. Appl. Phys. **50**, 4362 (1979).

[34]A. Mooradian and A. L. McWhorter, Phys. Rev. Lett. **19**, 849 (1967).

[35]H. L. Störmer, R. Dingle, A. C. Gossard, W. Wiegmann, and M. D. Sturge, Solid State Commun. **29**, 705 (1979).

[36]D. C. Tsui and R. A. Logan, Appl. Phys. Lett. **35**, 99 (1979).

[37]S. Das Sarma and J. J. Quinn, Phys. Rev. B **25**, 7603 (1982).

[38]R. A. Smith, *Wave Mechanics of Crystalline Solids* (Chapman and Hall, London, 1961), Chap. 4.

[39]D. Kirillov, C. Webb, and J. Eckstein, Appl. Phys. Lett. **49**, 1366 (1986).